

## Article

# Automatic Control of Chemolithotrophic Cultivation of *Cupriavidus necator*: Optimization of Oxygen Supply for Enhanced Bioplastic Production

Vera Lambauer <sup>1,2,\*</sup> , Alexander Permann <sup>1,3</sup> , Zdeněk Petrášek <sup>2</sup> , Vanja Subotić <sup>4</sup> , Christoph Hochenauer <sup>4</sup> , Regina Kratzer <sup>2,\*</sup>  and Markus Reichhartinger <sup>3</sup> 

<sup>1</sup> Austrian Centre of Industrial Biotechnology (ACIB), Krenngasse 37, A-8010 Graz, Austria

<sup>2</sup> Institute of Biotechnology and Biochemical Engineering, Graz University of Technology, NAWI Graz, Petersgasse 12/I, A-8010 Graz, Austria; z.petrasek@tugraz.at

<sup>3</sup> Institute of Automation and Control, Graz University of Technology, Inffeldgasse 21B, A-8010 Graz, Austria; markus.reichhartinger@tugraz.at

<sup>4</sup> Institute of Thermal Engineering, Graz University of Technology, Inffeldgasse 25B, A-8010 Graz, Austria; vanja.subotic@tugraz.at (V.S.); christoph.hochenauer@tugraz.at (C.H.)

\* Correspondence: veralambauer@acib.at (V.L.); regina.kratzer@tugraz.at (R.K.)

**Abstract:** Gas fermentation is an upcoming technology to convert gaseous substrates into value-added products using autotrophic microorganisms. The hydrogen-oxidizing bacteria *Cupriavidus necator* efficiently uses CO<sub>2</sub> as its sole carbon source, H<sub>2</sub> as electron donor and O<sub>2</sub> as electron acceptor. Surplus CO<sub>2</sub> is stored in microbial storage material poly-(R)-3-hydroxybutyrate. O<sub>2</sub> supply is the most critical parameter for growth and poly-(R)-3-hydroxybutyrate formation. A narrow O<sub>2</sub> optimum between ~0.2 and ~4 mg/L was previously reported. Here, a standard benchtop bioreactor was redesigned for autotrophic growth of *C. necator* on explosive mixtures of CO<sub>2</sub>, H<sub>2</sub> and O<sub>2</sub>. The bioreactor was equipped with mass flow control units and O<sub>2</sub> and CO<sub>2</sub> sensors. A controller for automated gas dosage based on a mathematical model including gas mass transfer, gas consumption and sensor response time was developed. Dissolved O<sub>2</sub> concentrations were adjusted with high precision to 1, 2 and 4% O<sub>2</sub> saturation (0.4, 0.8 and 1.5 mg/L dissolved O<sub>2</sub>, respectively). In total, up to 15 g/L cell dry weight were produced. Residual biomass formation was 3.6 ± 0.2 g/L under all three O<sub>2</sub> concentrations. However, poly-(R)-3-hydroxybutyrate content was 71, 77 and 58% of the cell dry weight with 1, 2 and 4% dissolved O<sub>2</sub>, respectively.

**Keywords:** CO<sub>2</sub> valorization; hydrogen oxidizing bacteria; Knallgas bacteria; gas fermentation; bioprocess control; polyhydroxyalkanoate



**Citation:** Lambauer, V.; Permann, A.; Petrášek, Z.; Subotić, V.; Hochenauer, C.; Kratzer, R.; Reichhartinger, M. Automatic Control of Chemolithotrophic Cultivation of *Cupriavidus necator*: Optimization of Oxygen Supply for Enhanced Bioplastic Production. *Fermentation* **2023**, *9*, 619. <https://doi.org/10.3390/fermentation9070619>

Academic Editor: Konstantinos G. Kalogiannis and Maria Antoniadou

Received: 1 June 2023  
Revised: 23 June 2023  
Accepted: 25 June 2023  
Published: 29 June 2023



**Copyright:** © 2023 by the authors. Licensee MDPI, Basel, Switzerland. This article is an open access article distributed under the terms and conditions of the Creative Commons Attribution (CC BY) license (<https://creativecommons.org/licenses/by/4.0/>).

## 1. Introduction

Reutilization of CO<sub>2</sub> as feedstock of chemicals and materials is the principal route towards a net-zero CO<sub>2</sub> emission economy. General utilization options are either direct use of CO<sub>2</sub> without chemical conversion (e.g., for enhanced oil recovery or food or beverage production) or chemical and biological CO<sub>2</sub> conversion into useful products [1–3]. The main biological assimilation pathways are phototrophic CO<sub>2</sub> fixation by plants, algae and cyanobacteria and lithotrophic CO<sub>2</sub> fixation by specialized bacteria [4,5]. The most efficient CO<sub>2</sub> assimilation into biomass has been reported for aerobic hydrogen-oxidizing bacteria (HOBs or Knallgas bacteria) [6–9]. HOBs assimilate CO<sub>2</sub> by using H<sub>2</sub> and O<sub>2</sub> as electron and energy donors, respectively, [10,11]. Amongst them, *Cupriavidus necator* (also known as *Ralstonia eutropha*) is considered a potential game changer in biological CO<sub>2</sub> utilization, as it is able to convert surplus CO<sub>2</sub> into the microbial storage material polyhydroxyalkanoate (PHA) [12]. PHAs are biodegradable thermoplasts and hold great potential as substitutes for bulk plastics such as polypropylene or polyethylene [13]. In balanced media, the

organism divides until one or more nutrients become limiting (biomass growth phase). Under nutrient-limiting conditions, the organism stores surplus CO<sub>2</sub> as short-chain-length PHA (poly-(R)-3-hydroxybutyrate, PHB) up to ≤80 % of its cell dry weight (PHA storage phase) [12,14]. Substrate gas mixtures contain H<sub>2</sub> as a major component and CO<sub>2</sub> and O<sub>2</sub> as minor components. The exact gas compositions vary in reported gas cultivations, but excesses of H<sub>2</sub> and CO<sub>2</sub> are generally used under O<sub>2</sub>-limiting conditions (as reviewed in [14]). The dissolved oxygen (dO<sub>2</sub>) concentration is considered the most critical process parameter in the chemolithotrophic cultivation of *C. necator* (and HOBs in general) from technical and biological points of view. The main technical challenge is that O<sub>2</sub> and H<sub>2</sub> form explosive oxyhydrogen mixtures with lower and upper explosion limits of 4.8 and 95.2% H<sub>2</sub>, respectively [15]. The low minimum ignition energy of 0.016 mJ classifies oxyhydrogen mixtures as highly flammable, and therefore, used cultivation experiments have to satisfy appropriate safety requirements [15]. Standard lab bioreactors cannot be used with explosive gases, as stirrer motors (mostly brush motors) and control electronics inside and outside of the bioreactor (sensors for O<sub>2</sub>, pH and temperature; pumps for acids, bases, water and control boards) constitute possible ignition sources. In practice, either bioreactors designed for long-term operation with explosive gas mixtures, i.e., in ex-zone 0 (Ex-zones are areas in which explosive atmospheres may occur. Depending on the time period during which an explosive mixture is present, a distinction is made between ex-zones 0, 1 and 2, with 0 being the longest time period—“constantly or frequently”). Regulations for Europe can be found in ATEX Product Directive 2014/34/EU and ATEX Operating Directive 1999/92/EC.), [14] or bioreactors with high gas mass transfer rates were used [16,17]. The main advantage of systems with high mass transfer rates is that a sufficient O<sub>2</sub> supply of the cells (dO<sub>2</sub> concentration) at low O<sub>2</sub> ratios in the substrate gas mixture are reached. Therefore, these bioreactors operate most of the time with gas mixtures outside the explosion limits. Since an ignitable gas mixture cannot be avoided in 100% here either, these bioreactors operate in the lower ex-zones (1 or 2). The safety regulations for equipment and operation are strictest in ex-zone 0. dO<sub>2</sub> concentrations for optimal growth were previously reported to range between 1.9 and 4 mg L<sup>-1</sup> [18]. During PHB accumulation, less O<sub>2</sub> is required, culminating in half-saturation constant for O<sub>2</sub>-dependent PHA formation of  $K_{pO_2} 1.8 \times 10^{-2} \text{ mgL}^{-1}$  [19]. Hence, fast-growing cultures have a highly dynamic O<sub>2</sub> demand and require precise control to keep the dO<sub>2</sub> concentration within a desired and narrow process-dependent narrow range. We recently published a continuous and cheap cultivation setup with manually adjusted O<sub>2</sub> supply over several days. Manual O<sub>2</sub> supply was guided by [14] and realized by in situ measurements of dO<sub>2</sub> concentration with an O<sub>2</sub> dipping probe. Despite the tedious and time-consuming manual work, the dO<sub>2</sub> concentration was frequently outside of the desired range [14]. Hence, there is a need for the automatic control of O<sub>2</sub> supply for convenient and reproducible cultivation of *C. necator*. In this paper, we propose a systematically designed model-based automatic regulation of O<sub>2</sub> and CO<sub>2</sub> for a bioreactor operating in zone 0 (In zone 0, a hazardous explosive atmosphere is frequently present during normal operation). The proposed model is supported by in situ measurements of O<sub>2</sub> and CO<sub>2</sub> using dipping probes. The model-based approach reported herein also enabled the design and implementation of uptake rate and disturbance estimators. As a result, the achieved closed-loop performance is improved additionally by allowing for the determination of the currently prevailing growth phase, i.e., the biomass growth phase or PHA accumulation phase. Experimental studies demonstrate that the proposed concept achieves accurate gas levels during the entire cultivation time.

## 2. Materials and Methods

### 2.1. Chemicals, Assays and Organisms

H<sub>2</sub> (purity 99.999%), O<sub>2</sub> (purity 99.999%), CO<sub>2</sub> (purity 99.5%) and N<sub>2</sub> (purity 99.999%) were purchased from Air Liquide Austria (Graz, Austria). Kanamycin sulfate (≥750 IU/mg, Art. No. T832.1) was from Carl Roth (purchased at Lactan, Graz, Austria). Poly-(R)-3-hydroxybutyric acid from Sigma Aldrich (quality level 200, Art. No. 363502, Vienna

Austria) was used as the standard for GC analysis. Other chemicals used in this study were from Sigma Aldrich or Carl Roth and purchased in the highest available purity. Concentrations of ammonia and fructose were measured using K-AIMAR and K-SURFG test kits from Megazyme International (Wicklow, Ireland). The strain *C. necator* H16 DSM 428 (aka ATCC 17699, NCIB 10442) was obtained from DSMZ, Deutsche Sammlung für Mikroorganismen und Zellkulturen.

## 2.2. Media and Inoculum

Stock cultures were stored in 2 mL free-standing cryovials with external threads (Art. No. E315.1, Carl Roth). They contained 0.75 mL of liquid culture in mineral media with 20 g L<sup>-1</sup> fructose and 0.75 mL of 1.8 M trehalose. Cryopreserved cells were reactivated on mineral media agar plates containing 20 g L<sup>-1</sup> fructose at 30 °C for 24 h [14]. Cells were used to inoculate 50 mL of mineral medium with 20 g L<sup>-1</sup> fructose in 300 mL baffled flasks. Precultures were incubated at 30 °C and 120 rpm in an orbital shaker for up to 24 h to capture the culture in the late exponential phase. All gas fermentations were performed in mineral media with CO<sub>2</sub> as the sole carbon source. Mineral media composition was described in a previous publication [14].

## 2.3. Safety Considerations

Personal and technical safety was considered according to ATEX directives RL 1999/92/EG and RL 2014/34/EU.

### 2.3.1. Room and Ventilated Hood

A schematic diagram of the setup used for gas cultivations is depicted in Figure 1. H<sub>2</sub>, O<sub>2</sub> and N<sub>2</sub> were supplied by gas lines from outside the used facility room. CO<sub>2</sub> was supplied from a gas bottle located in the room. The individual gas flow rates were adjusted online (LabVIEW program from National Instruments Corp., Austin, TX, USA) with the help of mass flow controllers (MFCs for H<sub>2</sub>, CO<sub>2</sub> and O<sub>2</sub> from Vögtlin Instruments GmbH, Muttens, Switzerland). Substrate gas mixtures were mixed on-site. The gas lines for the substrate gas feed (H<sub>2</sub>, O<sub>2</sub> and CO<sub>2</sub> premixed), the gas phase of the bioreactor and the off-gas line temporarily contained H<sub>2</sub> and O<sub>2</sub> in explosive mixtures (defined as ex-zone 0). The ventilated hood (Secuflow, Airflow Controller from Waldner GmbH & Co. KG, Wangen im Allgäu, Germany) provided a ventilation of 580 m<sup>3</sup>/h to dilute the off-gas approx. 10,000 times before it was blown out at the top of the building. The interior of the fume hood was considered to be an area where the occurrence of an explosive gas mixture was not likely or was likely to occur only for a short period of time due to the strong ventilation (defined as ex-zone 2). Note that due to the high diffusivity of H<sub>2</sub>, there might be a low concentration of H<sub>2</sub> in a close vicinity to the bioreactor (legally defined by default as zone 1, i.e., explosive atmospheres may occasionally form during normal operation). In practice, zone 1 is negligible because of the strong ventilated fume hood. A gas detector (detector ExTox Sens BG-WT from Gasmess-Systeme GmbH, Unna, Germany) was installed in the fume hood. H<sub>2</sub> detection would have triggered gas stoppage (closing of a magnetic check-valve type EPS 18 ATEX 1232 X from Bürkert, Ingelfingen, Germany), bioreactor stoppage (stopping of the motor of the bioreactor) and alarm signals (on-site and remote). The room had an antistatic floor.

### 2.3.2. Bioreactor Setup: Pipe and Flow Diagram of the Lab

A Labfors bioreactor with a double-walled 1.2 L reaction vessel (from Infors HT, Bottmingen, Switzerland) was redesigned for use in the ex-zone. All electrical parts from the Labfors bioreactor were removed. The agitator motor and water circulation thermostat were replaced by an external powerdrive three-phase motor (0.75 kW from Pfeiffer Elektromotoren, Vienna, Austria) and a Lauda water bath with a circulation pump (Dr. R. Wobser GmbH & CO. KG, Königshofen, Germany). All possible ignition sources were placed outside the ventilated hood. The brush motor was mounted above the hood, and the

shaft drive was elongated. The thermostat and the circulation pump were placed outside the hood, and the water tubes were elongated. No CO<sub>2</sub> probe certified for the ex-zone zero was available on the market. Therefore, we used a submersible CO<sub>2</sub>-dipping probe based on an optical fiber that was considered intrinsically safe according to the supplier (CD1-L2.5-St5-US from Presens GmbH, Regensburg, Germany). Read-out electronics of the CO<sub>2</sub> sensor probe were considered as possible ignition sources. Therefore, they were removed from the immediate vicinity of the bioreactor. The dissolved oxygen probe was a VisiFerm mA 225 H3 (Hamilton Bonaduz AG, Bonaduz, Switzerland) certified for use in the ex-zone (zone 0, category IIC, T4-6). The lid of the bioreactor and the sensors were grounded by connections to an equipotential socket in the hood to ensure that the whole fermentation plant was equipotentially balanced.

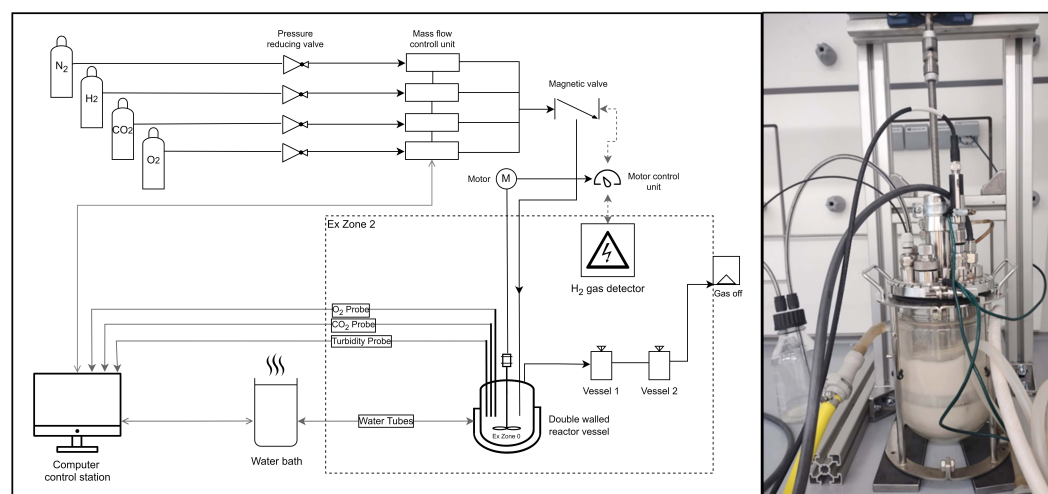


**Figure 1.** Schematic diagram of lab installations, the bioreactor equipped for gas cultivations and defined ex-zones (left). Image of the fermentation vessel during cultivation (right). (Open-source program diagrams.net © 2005–2021 JGraph Ltd. was used for figure preparation). Gas flow rates were regulated by mass flow controllers (MFCs). Statically mixed gas flowed into the bioreactor by passing through a magnetic valve. The magnetic valve was connected to the motor control unit, as well as the H<sub>2</sub> gas detector placed in the fume hood (ex-zone 2). In case of H<sub>2</sub> detection in ex-zone 2, the magnetic valve would be closed and the motor stopped. The bioreactor was equipped with a double-walled vessel for temperature control by a water bath, as well as O<sub>2</sub> and CO<sub>2</sub> sensors to measure dissolved gas concentrations in the liquid phase. MFCs, sensors and the temperature bath were connected to the computer and controlled via LabVIEW (National Instruments Corp.).

### 2.3.3. Personal Protective Measures

The researcher responsible for gas cultivation attended an explosion protection course at the TÜV AUSTRIA Academy (Graz, Austria). Personal protective equipment included safety glasses, an antistatic lab coat (Art. No. 88258, uvex SuXXeed ESD, UVEX Arbeitsschutz GMBH, Fürth, Germany) and antistatic shoes (Art. No. 7315, Abeba Dynamic, Schmuck Arbeitsschutzprodukte Vertriebs GmbH, Bad Salzungen, Germany). Additionally, the H<sub>2</sub> gas was switched off before the researcher entered the laboratory.

### 2.4. Operation of the Gas Cultivation System

The  $k_L a$  of the bioreactor was determined by the static gassing-out method [14]. Calibrations of the CO<sub>2</sub> and O<sub>2</sub> probes were achieved by two-point calibrations. Zero (0% dissolved O<sub>2</sub> or CO<sub>2</sub>) was determined by purging the reactor with N<sub>2</sub>. The oxygen probe was calibrated to 100% dissolved oxygen by purging the reactor with 100% pure O<sub>2</sub>. The CO<sub>2</sub> probe was calibrated to 20% dissolved carbon dioxide by purging the reactor with a gas mixture of 20% CO<sub>2</sub> and 80% N<sub>2</sub>. The Labfors cultivation vessel was autoclaved with the mounted dissolved oxygen dipping probe. Under sterile conditions, the chemically sterilized (ethanol 70% (v/v)) CO<sub>2</sub>-dipping probe was fitted into the reactor, and

the presterilized mineral medium (1 L) was added. Heterotrophically grown preculture was added aseptically through a septum (start  $OD_{600} \leq 1$ ). The filled bioreactor was connected to the substrate gas and off-gas lines. The tightness of the bioreactor and gas connections was checked with the purge gas  $N_2$  and a leak detector spray. Stirrer speed velocity and temperature were held constant at 887 rpm and 30 °C, respectively. Under chemolithotrophic conditions, dissolved  $CO_2$  and  $O_2$  were kept constant at 5% and 2%, respectively, by automation and control in LABVIEW.  $H_2$  was manually set constant at  $400 \text{ mL min}^{-1}$  to ensure an excess of dissolved hydrogen.  $N_2$  was used as a filling gas to ensure a total and constant gas supply rate of  $1 \text{ L min}^{-1}$ . Prior to sampling,  $H_2$  was set to 0% in the substrate gas mixture, and the bioreactor was purged with substrate gas lacking  $H_2$  for 10 min (flow rate of  $1 \text{ L min}^{-1}$ ). Sampling was performed using a syringe with a needle. The needle was inserted through a septum by opening a blind plug. After sampling, the blind plug was closed again, and the bioreactor tightness checked with the purge gas and a leak detector spray. Bioreactor cultivation was performed for 5–7 days. Biomass was harvested by centrifugation, and the supernatant and pellet were stored separately at  $-20 \text{ °C}$ .

### 2.5. Data Acquisition and Processing

Oxygen probe readings were gathered at a 2 s interval. The measured parameter was the dissolved oxygen ( $C_{O_2}$ ). The main program cycle used to estimate uptake rates and adjust inlet gas compositions was executed every 2 s according to the presented control laws. The  $CO_2$  probe was prone to light-induced aging of the reactive dye in the sensor membrane. Therefore, the  $CO_2$  measurement intervals were increased to 300 s to maintain reliable probe readings throughout the cultivation experiment. The measured parameter was the dissolved  $CO_2$ . Read-outs of gas probes were presented as % saturation, and 100% and 0% saturations were obtained by purging the aqueous media with the respective pure gas ( $O_2$  or  $CO_2$ ) and  $N_2$ , respectively.

### 2.6. Analytics

#### 2.6.1. Optical Density and Cell Dry Mass

Optical densities of culture broth samples were measured at 600 nm ( $OD_{600}$ ). Mineral medium was used as a blank reading and, if necessary, to dilute the samples. Cell dry mass was determined using the volumetric method with drying of the biomass at 105 °C as described previously [14].

#### 2.6.2. PHA Determination

PHA was extracted from lyophilized cells by a multistep method. First, ethanol was added to dissolve lipids. Then, ethanol and dissolved lipids were removed by centrifugation, and the remaining pellet was dried. PHA was extracted with chloroform from the degreased pellet. Finally, PHA was precipitated by the addition of ice-cold ethanol, subsequently concentrated by filtration and dried. Methanolysis of PHA was performed in order to determine the PHA content by GC. The GC was equipped with a ZB-5 column (Phenomenex; 30 m length; 0.32 mm inner diameter; 0.25  $\mu\text{m}$  film thickness) and an FID detector. PHA determination was previously described in detail [14,20].

## 3. Theory/Calculation

In this section, we present a mathematical model and a controller design for the purpose of automatically regulating  $O_2$  and  $CO_2$  concentrations.

### 3.1. Mathematical Modelling and Automatic Control Problem Formulation

The dynamics of the dissolved concentrations of O<sub>2</sub> and CO<sub>2</sub> in the fermentation broth are assumed to be captured by

$$\frac{dC_i}{dt} = N_i + \Theta_i - Q_i, \quad (1)$$

where  $C_i$  denotes the dissolved concentration in %,  $N_i$  covers the gas-to-liquid mass transfer rate in % s<sup>-1</sup>,  $\Theta_i$  represents the impact of the considered chemical reactions in % s<sup>-1</sup> and  $Q_i$  refers to remaining non-modeled effects mainly caused by the bacterial uptake rate in % s<sup>-1</sup>. Note that this model structure is applied to the concentrations of both O<sub>2</sub> and CO<sub>2</sub>; hence,  $i \in \{O_2, CO_2\}$ .

Gas-to-liquid mass transfer is modeled using the two-film theory [21,22]. Hence, it is assumed that the mass transfer is proportional to the difference in concentrations of the gaseous state and the dissolved state. The concentration in the gaseous state refers to the fraction of the respective gas within the inlet gas composition. A sufficiently fast exchange of gas inside the bioreactor is assumed; hence, the gas concentrations can be directly adjusted by the mass flow controllers. The dissolved concentration, on the other hand, refers to the maximum solubility of the respective gas in the fermentation broth. Consequently, for each gas, a dissolved liquid concentration of 100% is reached after applying a 100% inlet gas concentration of the respective gas for a sufficiently long time. The mass transfer from gas to liquid is modeled by

$$N_i = k_L a_i (C_i^* - C_i), \quad (2)$$

where  $k_L a_i$  represents a transfer-rate coefficient in s<sup>-1</sup>, which depends on the total inlet gas flow ( $u_1$ ) given in mL min<sup>-1</sup>. The transfer rate coefficient is approximated by

$$k_L a_i(u_1) = \alpha_i u_1 + \beta_i. \quad (3)$$

where  $\alpha_i$  and  $\beta_i$  denote liquid-dependent positive constants. Furthermore, the respective gas concentration is labeled by  $C_i^*$  and is given in %. Note that the temperature impact on  $k_L a$  is neglected. This is motivated by the assumption that the temperature is kept constant by the temperature bath during the fermentation. The variations in the liquid properties that may influence the transfer rate coefficient ( $k_L a$ ) during the process are neglected.

The effect of chemical reactions takes into account CO<sub>2</sub> only, since O<sub>2</sub> does not react with H<sub>2</sub>O. The reaction of CO<sub>2</sub> with H<sub>2</sub>O triggers a series of reversible reactions, forming a so-called buffer system. CO<sub>2</sub> first reacts to carbonic acid, as described by



and further to bicarbonate, as expressed by



which eventually yields



The reaction's equilibrium depends on the pH value of the liquid. In this process, the pH value is kept constant by the addition of a phosphate buffer, ensuring a pH value between 6.5 and 7.0. No further pH control or adjustment during fermentation was necessary. The chemical reaction shown in reaction (6) is omitted in the presented mathematical

model, since the concentration of  $\text{CO}_3^{2-}$  is negligibly small at the given pH value [23]. The dynamics of reversible reactions (4) and (5) are modeled by

$$\frac{d}{dt}[\text{HCO}_3^-] = k_1 C_{\text{CO}_2} - k_{-1}[\text{H}^+][\text{HCO}_3^-] \tag{7}$$

to describe the time evolution of the bicarbonate concentration. The square brackets denote the respective concentration in the liquid, and  $k_1$  and  $k_{-1}$  denote constant reaction-rate coefficients. The concentrations of  $\text{H}^+$  ions can be calculated from the known pH level ( $p$ ) and by replaced by the constant  $k_H = 10^{-p}$ .

The dynamic conversion of  $\text{CO}_2$  shown in Equation (7) describes the reduction in the  $\text{CO}_2$  concentration in the fermentation broth. Given the reversible nature of the considered process, increasing the  $\text{HCO}_3^-$  concentration results in an increase in  $\text{CO}_2$  as well. This coupling effect is modeled by

$$\Theta_{\text{CO}_2} = -k_1 C_{\text{CO}_2} + k_{-1} k_H [\text{HCO}_3^-] \tag{8}$$

The terms  $Q_{\text{O}_2}$  and  $Q_{\text{CO}_2}$  are not mathematically modeled in this paper, while  $Q_{\text{O}_2}$  refers to the bacterial oxygen uptake rate,  $Q_{\text{CO}_2}$  includes several parameters due to the dependence of  $\text{CO}_2$  solubility on pH, temperature and ionic strength. During fermentation, slight pH changes in a range of 6.5–7.0 may occur as ions are consumed by bacteria. Therefore, pH, as well as ionic strength, may differ over time [24]. In addition, metabolites from the cells are exported into the aqueous solution, which also changes the ionic strength [25]. In comparison with the dynamic effects described above, the individual  $\text{O}_2$  and  $\text{CO}_2$  uptake rates are assumed to be time-dependent and changing with a variety of process parameters and with the current biomass growth phase. From a control engineering point of view, they are regarded as a disturbance later on.

Introducing the state variables  $x_1, x_2, x_3$  and  $x_4$  and the input variables  $u_1, u_2$  and  $u_3$ , as explained in Table 1, yields the overall dynamic model.

$$\frac{d}{dt} x_1 = k_L a_{\text{O}_2}(u_1)(u_2 - x_1) - Q_{\text{O}_2}, \tag{9a}$$

$$\frac{d}{dt} x_2 = k_L a_{\text{CO}_2}(u_1)(u_3 - x_2) - k_1 x_2 + k_{-1} k_H x_3 - Q_{\text{CO}_2}, \tag{9b}$$

$$\frac{d}{dt} x_3 = k_1 x_2 - k_{-1} k_H x_3, \tag{9c}$$

$$\frac{d}{dt} x_4 = \zeta(x_2 - x_4), \tag{9d}$$

with

$$k_L a_{\text{O}_2}(u_1) = \alpha_{\text{O}_2} u_1 + \beta_{\text{O}_2} \quad \text{and} \quad k_L a_{\text{CO}_2}(u_1) = \alpha_{\text{CO}_2} u_1 + \beta_{\text{CO}_2}. \tag{10}$$

Note that in the proposed mathematical model (9), the dynamics of the  $\text{CO}_2$  concentration measurement transducer are also considered by a lag element represented by (9d) with time constant  $\zeta^{-1}$ . In the case of the  $\text{O}_2$  probe, i.e., the measurement of  $x_1$ , the introduction of additional dynamics was not required.

The overall goal of the controller design presented in Section 3.2 is to adjust  $u_1, u_2$  and  $u_3$  in such a manner that the dissolved concentrations of  $\text{O}_2$  and  $\text{CO}_2$ , i.e.,  $x_1$  and  $x_2$ , respectively, approach the constant given levels ( $r_i$ ).

**Table 1.** Description of the variables of the O<sub>2</sub>-CO<sub>2</sub> mass transfer model. (\* Disturbances).

	Variable	Explanation
States	$x_1$	O <sub>2</sub> dissolved concentration
	$x_2$	CO <sub>2</sub> dissolved concentration
	$x_3$	HCO <sub>3</sub> <sup>-</sup> concentration
	$x_4$	CO <sub>2</sub> probe reading
Inputs	$u_1$	Total inlet gas flow $q_{ges}$
	$u_2$	O <sub>2</sub> concentration in the inlet gas $C_{O_2}^*$
	$u_3$	CO <sub>2</sub> concentration in the inlet gas $C_{CO_2}^*$
Parameters	$k_L a_i$	O <sub>2</sub> or CO <sub>2</sub> mass transfer rate coefficient as a function of $u_1$
	$\alpha_i, \beta_i$	O <sub>2</sub> or CO <sub>2</sub> $k_L a$ model parameters
	$k_1$	Reaction rate from CO <sub>2</sub> to HCO <sub>3</sub> <sup>-</sup>
	$k_{-1}$	Reverse reaction rate from HCO <sub>3</sub> <sup>-</sup> to CO <sub>2</sub>
	$k_H$	pH-dependent constant
	$\xi$	Reciprocal of the CO <sub>2</sub> probe reading time constant
Dis *	$Q_{O_2}$	O <sub>2</sub> estimator
	$Q_{CO_2}$	CO <sub>2</sub> estimator

### 3.2. Controller Design

The design of the controllers relies on the assumption that the total mass flow ( $u_1$ ) is specified by the bioreactor’s operator. Therefore, it is known and should not be adjusted automatically by the automatic control algorithms designed in this section. Furthermore, the reference signals ( $r_i$ ) are assumed to be constant. Any sensor dynamics are neglected for the design of the controllers as well. The rates ( $Q_i$ ) are regarded as slowly (More precisely, the dynamics of  $Q_i$  are regarded significantly slower than the dynamics of dissolved concentrations of O<sub>2</sub> and CO<sub>2</sub> captured by (9a) and (9b)) time-varying. In a first step of the controller design, it is also assumed that the functions ( $Q_i$ ) are known. This assumption is relaxed in Section 3.2.4 when estimators are presented.

Both the O<sub>2</sub> controller design and the CO<sub>2</sub> controller design rely on the definition of the tracking error.

$$e_i = r_i - x_i, \tag{11}$$

where  $r_{O_2}$  and  $r_{CO_2}$  denote the constant O<sub>2</sub> and CO<sub>2</sub> reference, respectively. Figure 2 shows an overview of the control system and its individual components presented in the following subsections. Values for the total flow ( $u_1$ ), the H<sub>2</sub> flow and the reference signals are chosen directly by the operator. The O<sub>2</sub> and CO<sub>2</sub> controllers compute  $u_2$  and  $u_3$ , which allows for the calculation of the respective flow rates that are passed on to the mass flow controllers.

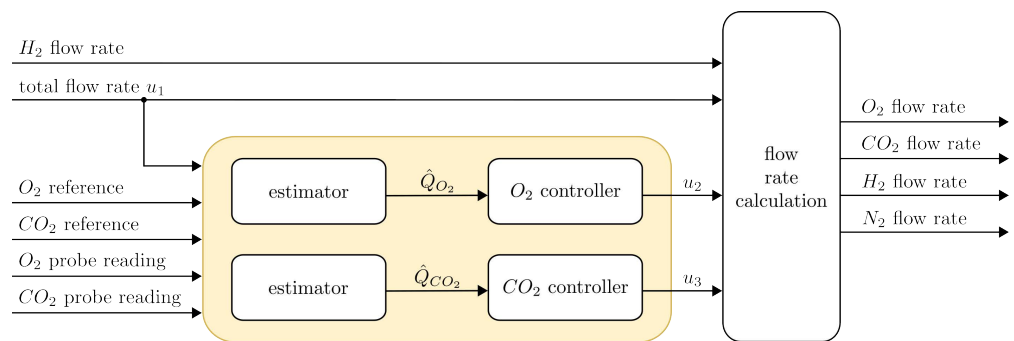


**Figure 2.** Overview of the control scheme with O<sub>2</sub> and CO<sub>2</sub> estimators.

#### 3.2.1. O<sub>2</sub> Controller

Computing the dynamics of the tracking error ( $e_1$ ) yields

$$\frac{de_1}{dt} = -k_L a_{O_2}(u_1)(u_2 - x_1) + Q_{O_2}, \tag{12}$$

where  $u_2$  is regarded as the  $O_2$  controller’s control signal. Prescribing the above tracking error dynamics by

$$\frac{de_1}{dt} = -k_{O_2}e_1 \quad \text{with} \quad k_{O_2} > 0 \tag{13}$$

allows Equations (12) and (13) to be solved and for the control signal to be rearranged.

$$u_2 = \frac{k_{O_2}e_1 + Q_{O_2}}{k_L a_{O_2}(u_1)} + x_1. \tag{14}$$

It is interesting to note that the control signal ( $u_2$ ) is automatically adjusted depending on the total flow ( $u_1$ ), which is selected such that no singularity occurs in the computation of  $u_2$ . The presented model-based design of control law (14) can easily be extended towards dynamic controllers by adopting the prescribed error dynamics shown in Equation (13). This allows for systematic generation of standard regulators such as PID controllers [26]. However, in experimental studies, the presented control algorithm was found to be capable of achieving the desired tracking error accuracy. Furthermore, the  $O_2$  control algorithm presented in Equation (14) can easily be implemented in discrete-time operated control hardware. Note that due to static control action, no antiwindup method needs to be implemented [27]. The discretized control algorithm is given by

$$u_{2,n} = \frac{k_{O_2}e_{1,n} + \hat{Q}_{O_2,n}}{k_L a_{O_2,n}} + x_{1,n}, \tag{15}$$

where  $e_{1,n} = r_{O_2} - x_{1,n}$  with  $x_{1,n} = x_1(nT_d)$ , the constant discretization time  $T_d$  and  $n = 0, 1, 2, \dots$ . In this discrete time realization of the control law, the uptake rate ( $Q_{O_2}$ ) is already replaced by its discrete time estimate ( $\hat{Q}_{O_2,n}$ ) presented in Section 3.2.4.

### 3.2.2. $CO_2$ Controller

The design of the  $CO_2$  controller also follows the method of prescribing the tracking error dynamics. Hence, the same method as in the previously presented  $O_2$  controller development is applied. However, a more sophisticated specification of the error dynamics was required to obtain the desired closed feedback loop tracking performance. More precisely, the tracking error,

$$e_2 = r_{CO_2} - x_2, \tag{16}$$

which is governed by

$$\frac{de_2}{dt} = -k_L a_{CO_2}(u_1)(u_3 - x_2) + k_1x_2 - k_{-1}k_hx_3 + Q_{CO_2}, \tag{17}$$

is specified to follow the total flow-dependent dynamics:

$$\frac{de_2}{dt} = -(k_{CO_2} + k_L a_{CO_2}(u_1))e_2, \tag{18}$$

where  $k_{CO_2}$  is a positive constant tuning parameter. Note that

$$k_{CO_2} + k_L a_{CO_2}(u_1) > 0 \tag{19}$$

ensures that the error ( $e_2$ ) vanishes as time tends toward infinity. This inequality holds within the admissible range of the flow ( $u_1$ ). In contrast to the  $O_2$  control loop, this design takes into account the fact that the dynamics of the  $CO_2$  concentration vary with the total

flow ( $u_1$ ). In particular, the tracking error convergence rate is “large” if the total flow ( $u_1$ ) is “high”. On the other hand, slow convergence is adjusted for “low” total flow situations. For the calculation of the control law ( $u_3$ ), the Equations (17) and (18) are equated, and the definition of the error ( $e_2 = r_{CO_2} - x_2$ ) is used. Rearranging for  $u_3$  yields the following control law:

$$u_3 = \frac{k_{CO_2}e_2 + k_1x_2 - k_{-1}k_hx_3 + Q_{CO_2}}{k_La_{CO_2}(u_1)} + r_{CO_2}. \tag{20}$$

This control law is, as in the  $O_2$  control case, a static relation, and the implementation as a discrete time control law is straightforward. However, taking into account the measurement time interval of the  $CO_2$  probe mentioned in Section 2.5 allows for further simplification of the control law. The equilibrium of the bicarbonate buffer dynamics from Equation (9c) is characterized by

$$0 = k_1x_2 - k_{-1}k_hx_3 \Rightarrow k_1x_2 = k_{-1}k_hx_3. \tag{21}$$

As a consequence of this steady-state consideration of the bicarbonate buffer, the following control law results:

$$u_3 = \frac{k_{CO_2}e_2 + Q_{CO_2}}{k_La_{CO_2}(u_1)} + r_{CO_2} \tag{22}$$

The corresponding discrete time realization including the  $CO_2$  estimator ( $\hat{Q}_{CO_2,n}$ ) from Section 3.2.4 is given by

$$u_{3,n} = r_{CO_2} + \frac{k_{CO_2}e_{2,n} + \hat{Q}_{CO_2,n}}{k_La_{CO_2}(u_{1,n})} \tag{23}$$

where  $e_{2,n} = r_{CO_2} - x_{2,n}$  with  $x_{2,n} = x_2(nT_d)$ .

### 3.2.3. Flow Rate Calculation

Control laws (15) and (23) provide the fractions of  $O_2$  and  $CO_2$  in the inlet gas composition. Besides  $O_2$  and  $CO_2$ , the inlet gas composition contains  $H_2$  and  $N_2$ . The flow rate of  $H_2$ , i.e.,  $q_{H_2}$ , is directly chosen by the operator, while the  $N_2$  flow rate ( $q_{N_2}$ ) is used as a filling gas to maintain the desired concentrations. The actual flow rates can therefore be calculated as

$$q_{O_2} = u_1 u_{2,n} , \tag{24}$$

$$q_{CO_2} = u_1 u_{3,n} , \tag{25}$$

$$q_{N_2} = u_1 - q_{O_2,n} - q_{CO_2,n} - q_{H_2,n} , \tag{26}$$

where  $u_1$  represents the total flow rate, as defined by the operator.

### 3.2.4. Estimator Design

The estimators are based on a steady-state assumption for which all dynamics of the mass transfer, the bicarbonate buffer and the probe reading are settled. Equations (9a)–(9d) in a steady state are given by

$$0 = k_La_{O_2}(u_1)(u_2 - x_1) - Q_{O_2}, \tag{27a}$$

$$0 = k_La_{CO_2}(u_1)(u_3 - x_2) - k_1x_2 + k_{-1}k_hx_3 - Q_{CO_2}, \tag{27b}$$

$$0 = k_1x_2 - k_{-1}k_hx_3, \tag{27c}$$

$$0 = \xi(x_2 - x_4) , \tag{27d}$$

which further simplifies to

$$0 = k_L a_{O_2}(u_1)(u_2 - x_1) - Q_{O_2}, \tag{28a}$$

$$0 = k_L a_{CO_2}(u_1)(u_3 - x_4) - Q_{CO_2}. \tag{28b}$$

The similarity of Equations (28a) and (28b) allows suitable estimators to be derived for  $Q_{O_2}$  and  $Q_{CO_2}$  based on the follow general formulation:

$$0 = k_L a(u_1)(u_j - x) - Q, \tag{29}$$

with  $j \in \{2, 3\}$ , and  $x$ ,  $k_L a$  and  $Q$  are replaced, respectively, for  $O_2$  and  $CO_2$ . Rewriting Equation (29) yields the uptake rate:

$$Q = k_L a(u_1)(u_j - x). \tag{30}$$

Note that all quantities on the right-hand side of Equation (30) are known either by measurement or due to the control algorithms. In order to account for the slowly time-varying uptake rates and model inaccuracies, a recursive least squares estimation of the individual uptake rates is proposed in this paper. Defining the error ( $\epsilon$ ) as the deviation of the uptake rate ( $Q$ ) relative to its corresponding estimate  $\hat{Q}$ , i.e.,

$$\epsilon = Q - \hat{Q} = k_L a(u_1)(u_j - x) - \hat{Q}, \tag{31}$$

allows for computation of the estimated uptake rates by minimizing the cost function,

$$J = \min_{\hat{Q}} \epsilon^2, \tag{32}$$

with respect to  $\hat{Q}$ . This least squares optimization problem is solved by the recursive algorithm

$$\hat{Q}_{n+1} = \hat{Q}_n + k_Q \cdot \epsilon \tag{33}$$

$$= \hat{Q}_n + k_Q(Q - \hat{Q}_n) \tag{34}$$

$$= \hat{Q}_n + k_Q(k_L a(u_1)(u_j - x) - \hat{Q}_n), \tag{35}$$

given an initial rate ( $\hat{Q}_0$ ) and a constant tuning parameter ( $k_Q$ ) (see, e.g., [28]). The algorithm eventually converges to

$$\lim_{n \rightarrow \infty} \hat{Q}_n = Q, \tag{36}$$

assuming that the estimator iterates sufficiently rapidly compared to the volatility of the actual bacterial uptake rate.

### 3.2.5. Parameter Identification

The parameters given in Table 2 were verified with the help of the Matlab (Copyright 1990–2020 The MathWorks, Inc.) software package. Several experiments were conducted in the lab by applying various inlet gas compositions to the bioreactor while measuring the dissolved concentrations of  $O_2$  and  $CO_2$  inside the fermentation broth. The measured results were then compared with the simulation results of the model (see Section 3.1). Least squares optimization, which minimizes the error between the measurement results and the simulation output, was performed to determine the optimal set of model parameters listed in Table 2.

**Table 2.** Identified parameters of the proposed model (9).

O <sub>2</sub> model	$\alpha_{O_2}$	$\beta_{O_2}$			
		0.0822	9.4149		
CO <sub>2</sub> model	$\alpha_{CO_2}$	$\beta_{CO_2}$	$k_1$	$k_{-1}$	$\zeta$
		0.1440	-1.2616	0.0185	$6.4943 \cdot 10^4$

### 3.2.6. Controller Parameters

The derived controllers were implemented together with the identified model in Matlab and Simulink. The simulation allowed identified the appropriate initial values for the estimation and control parameters ( $k_{Q,O_2}$ ,  $k_{Q,CO_2}$ ,  $k_{O_2}$  and  $k_{CO_2}$ ). These parameters were then fine-tuned during preliminary experiments on the fermenter in order to optimize for rise time, stability and tracking performance. The parameters used in the fermentation experiment (see 4) are shown in Table 3.

**Table 3.** Identified controller parameters.

$k_{O_2}$	$k_{CO_2}$	$k_{Q,O_2}$	$k_{Q,CO_2}$
0.02	0	0.0001	0.0001

## 4. Results

Automatic control of chemolithotrophic fermentations is a key element to provide constant growth conditions for reproducible cultivation results. Elements of the setup reported herein included a standard bioreactor adapted for use in ex-zone 0 (removal of all possible ignition sources from the bioreactor and its immediate environment) and an automated controller of gas supply. The installation of an accurate controller with low deviations from target values requires tests of sensors without the biologic system and development of a mathematical model including gas mass transfer, gas consumption and sensor response time (in the case of CO<sub>2</sub>). After implementation of the control system, fermentations were performed under controlled conditions. Fine tuning of dissolved O<sub>2</sub> concentrations facilitated a detailed study on the influence of dissolved O<sub>2</sub> on growth and PHB production.

### 4.1. Parameter Identification

The proposed mathematical model (9) consisted of the parameters listed in Table 2, which were identified using measurement data (see Section 3.2.5). As an evaluation of the obtained mathematical model, known inlet gas mixtures were supplied to the reactor, and the dissolved concentrations of O<sub>2</sub> and CO<sub>2</sub> were measured with sensor probes inside the fermentation broth. Using the presented model parameters, a comparison between data obtained by measurement and simulation was carried out. As shown in Figure 3, the measured and simulated dissolved gas concentrations are in close accordance. The deviations between measurement data and simulation results for the dissolved O<sub>2</sub> are approximately 1% up to a gas concentration of 75% O<sub>2</sub> in the gas phase (a maximal error of ±3% was experienced at O<sub>2</sub> concentrations of 100% O<sub>2</sub> in the gas phase). The agreement between measured and simulated values of dissolved CO<sub>2</sub> was higher for gas concentrations of 15% CO<sub>2</sub> (error below 1%). The results for the CO<sub>2</sub> simulation were less accurate for higher CO<sub>2</sub> concentrations in the gas mixture. The dissolved CO<sub>2</sub> concentration was overestimated by 4% at an CO<sub>2</sub> concentration of 25% in the gas mixture. However, as maximal CO<sub>2</sub> concentrations of 10% were previously used in experiments and the model captures the main dynamics of the process, the model is regarded as sufficiently accurate to serve as the basis for the design of model-based control algorithms.

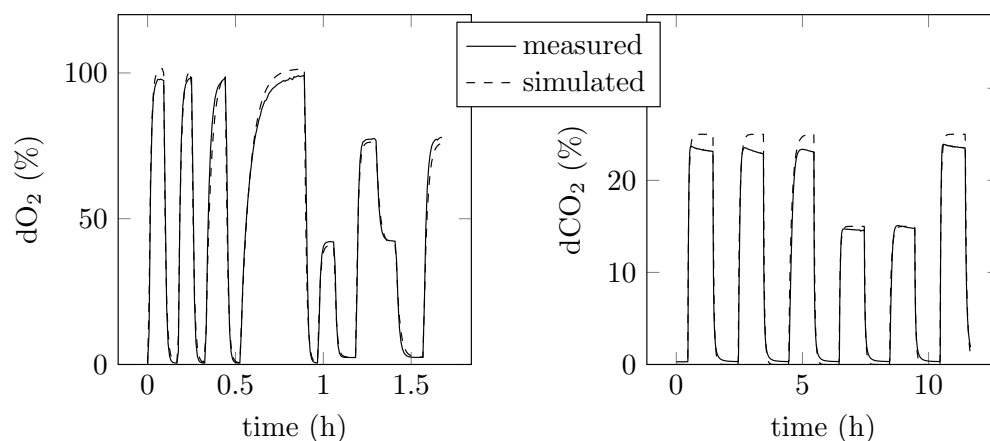


**Figure 3.** Results of parameter identification for the dissolved oxygen ( $dO_2$  in %) and dissolved carbon dioxide ( $CO_2$  in %) models.

#### 4.2. Experimental Evaluation

##### 4.2.1. Fermentation Results and PHB Output

We previously reported a simple gas fermentation setup with manual  $O_2$  supply lacking temperature and pH control. Growth curves of *C. necator*, biomass concentrations and PHB content obtained in the used 1 L stirred jar reactor were highly reproducible. However, manual adaptation of gas flow rates was restricted to personal effort, and the accuracy of manual dosage was limited [14]. The obtained growth curves including cell dry weights and PHB contents were in agreement with results of the cultivations reported herein with the same *C. necator* strain and the same medium composition. The change in temperature from room temperature (22–24 °C [14]) to 30 °C (this study Figure 4) did not seem to impact growth. A comparison of growth curves obtained with automatically controlled or manually supplied  $O_2$  can be found in the Supplementary Data (Supplementary Figure S1). Furthermore, the change from gentle mixing (340 rpm) with a magnetic anchor stirrer in a Duran glass bottle to maximum speed (887 rpm) with a Rushton turbine in a baffled bioreactor did not affect the cells. Shear stress response of small microbial cells is highly unlikely, as *C. necator* has a maximal length of about 1.3  $\mu\text{m}$  [16,25]. The difference in mixing efficiency was reflected in the  $k_L a$  values obtained with the used bioreactors. The previously used stirred Duran bottle had a  $k_L a$  value of 33  $\text{h}^{-1}$  at 340 rpm and a gas flow of 400  $\text{NmL}/\text{min}$ , while the Labfors bioreactor had a  $k_L a$  value of 110  $\text{h}^{-1}$  at 887 rpm and a gas flow of 1000  $\text{NmL}/\text{min}$  (measured with the “static gassing-out” method [14]). The higher  $k_L a$  value in the Labfors bioreactor allowed the use of lower  $O_2$  concentrations in the gas mixture, achieving sufficient  $O_2$  supply (2). The maximally required  $O_2$  content in the stirred Duran bottle was 21%, whereas with the Labfors, 8% was sufficient (Supplementary Figure S2). Therefore, the risk of explosion was significantly reduced, as the explosion pressure and rate are directly connected to  $O_2$  availability. Unfortunately, 887 rpm represented the maximal impeller speed from a technical point of view.

##### 4.2.2. Data and Controller Performance

The performance of the controllers and estimators is shown by the experimental results presented in Figure 5. Note that the spikes in the individual subplots of Figure 5 occur due to measurement sampling events, as during sampling, the  $H_2$  gas flow was switched off. The control errors of both the  $O_2$  controller and the  $CO_2$  controller were negligibly small during the entire course of the experiment. This can be seen in the zoomed-in plots (located in the individual plots) of the control error evolutions. Hence, the measured  $O_2$  and  $CO_2$  values were close to their reference values. The estimated uptake rate with respect to the  $O_2$  dynamics also indicates reasonable behavior. Under non-limiting conditions, gas cultivation up to 2.8  $\text{mmol L}^{-1}$  per CDW per hour (87  $\text{mg O}_2$  per CDW per hour) was utilized by the cells. This is slightly lower than that reported by Lu and Yu 2017 [29], who

obtained values between 4.4 and 85 mmol per CDW per hour depending on the limiting gas ( $H_2$ ,  $O_2$  or  $CO_2$ ). Looking into  $O_2$  inlet gas concentrations and OUR, it is possible to track the different growth phases of *C. necator* (Figure 5). In the first hours, remaining fructose from preculture was consumed, as evidenced by a rapid increase in  $O_2$  inlet gas flow concentration. Afterwards, the flow rate decreased as cells changed their metabolism to adapt to the new chemolithotrophic environment. The end of the lag phase was detected by a further increase in OUR and  $O_2$  concentration. N limitation was detected, as OUR stagnated (after approx. 30 h, Figure 5) when cells could no longer divide and started to store PHB. Over time, less  $O_2$  is needed to hold the desired level, as cells need less  $O_2$  during the PHB storage phase as they enter resting mode (PHB saturation). The evolution of the estimation of  $Q_{CO_2}$  showed negative values throughout the entire experiment, indicating that the uptake rate with respect to  $CO_2$  was dominated by the sum of other effects, such as inaccuracies in the model of  $k_L a_{CO_2}(u_1)$ , the neglected effect of sensor drift and a violation of the bicarbonate buffer steady-state assumption used in the development of the estimator. The time evolution of the automatically computed inlet gases is depicted in the lower plots in Figure 5. The controllers computed reasonable control actions, which were realized by the controlled valves. Furthermore, the spikes due to sampling events when  $H_2$  gas flow was switched off did not deteriorate the control loop performance. Note that this would not be the case if dynamic control algorithms without antiwindup methods were applied.

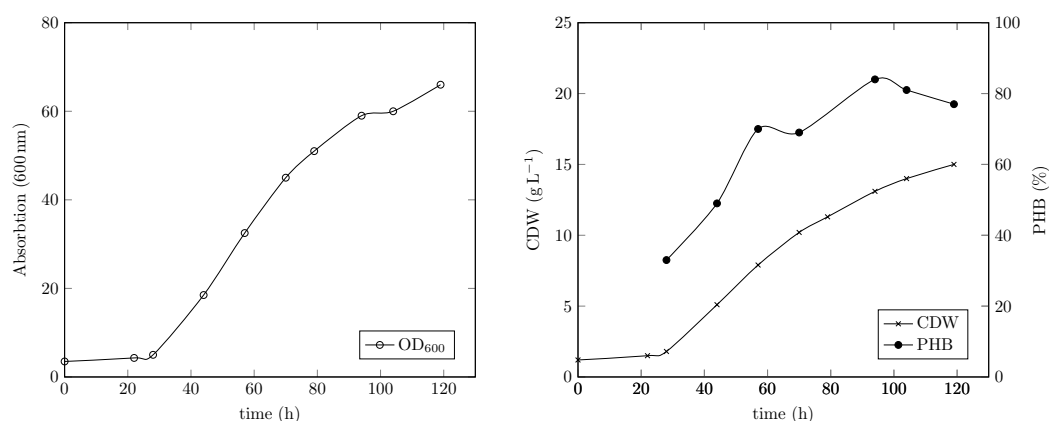


**Figure 4.** Cell density is provided in terms of optical density at 600 nm ( $OD_{600}$ ). Cell dry weight (CDW) is given in g. PHB is given in % relative to CDW.

#### 4.2.3. Gas Fermentation at Different $dO_2$ Concentrations

During microbial batch and fed-batch cultivations, substrate uptake kinetics gradually changed with the increase in biomass. Furthermore, sudden changes may occur when, e.g., substrates are added or samples are withdrawn. The supply of  $O_2$  (and of other gases) to bioreactors can be manipulated by the gas content in the feed gas mixture, the gas flow rate, the reactor pressure and the stirrer speed. Standard benchtop bioreactors use conventional control algorithms such as PID connected to an agitation and airflow control cascade for the control of  $O_2$ , pH and other parameters [30].  $O_2$  demand is highly dynamic. The most-often cultivated fast-growing microbes (*Escherichia coli* and yeasts) are facultative anaerobes, i.e., they survive under aerobic and anaerobic conditions. Hence, oxygen limitation leads to slower growth but not to culture loss of facultative anaerobes. For growth and PHB production of *C. necator* under heterotrophic conditions, optimal dissolved oxygen concentrations of 40% (3.17 mg/L) and 20% (1.59 mg/L) air saturation were previously reported [31]. Sonnleitner et al. (1979) showed that oxygen concentrations  $>2.8$  mg/L reduce growth and PHB production of *C. necator* H16 with lactic acid or  $CO_2$  as the carbon source [18]. Hence, it has been suggested that a general optimum for the  $dO_2$  concentration is independent of the carbon source. Higher  $O_2$  sensitivity of *C. necator* under chemolithotrophic growth conditions was attributed to  $O_2$  inhibition of the involved [NiFe]-hydrogenases [32]. We previously used an oxygen concentration of less than 5%

$dO_2$  (1.89 mg/L) [14]. However, the number of biotechnological labs equipped for tightly controlled Knallgas fermentations is restricted [17,30,33–35]. More often, *C. necator* is grown in closed bottles that are flushed with gases once or twice a day [36,37].

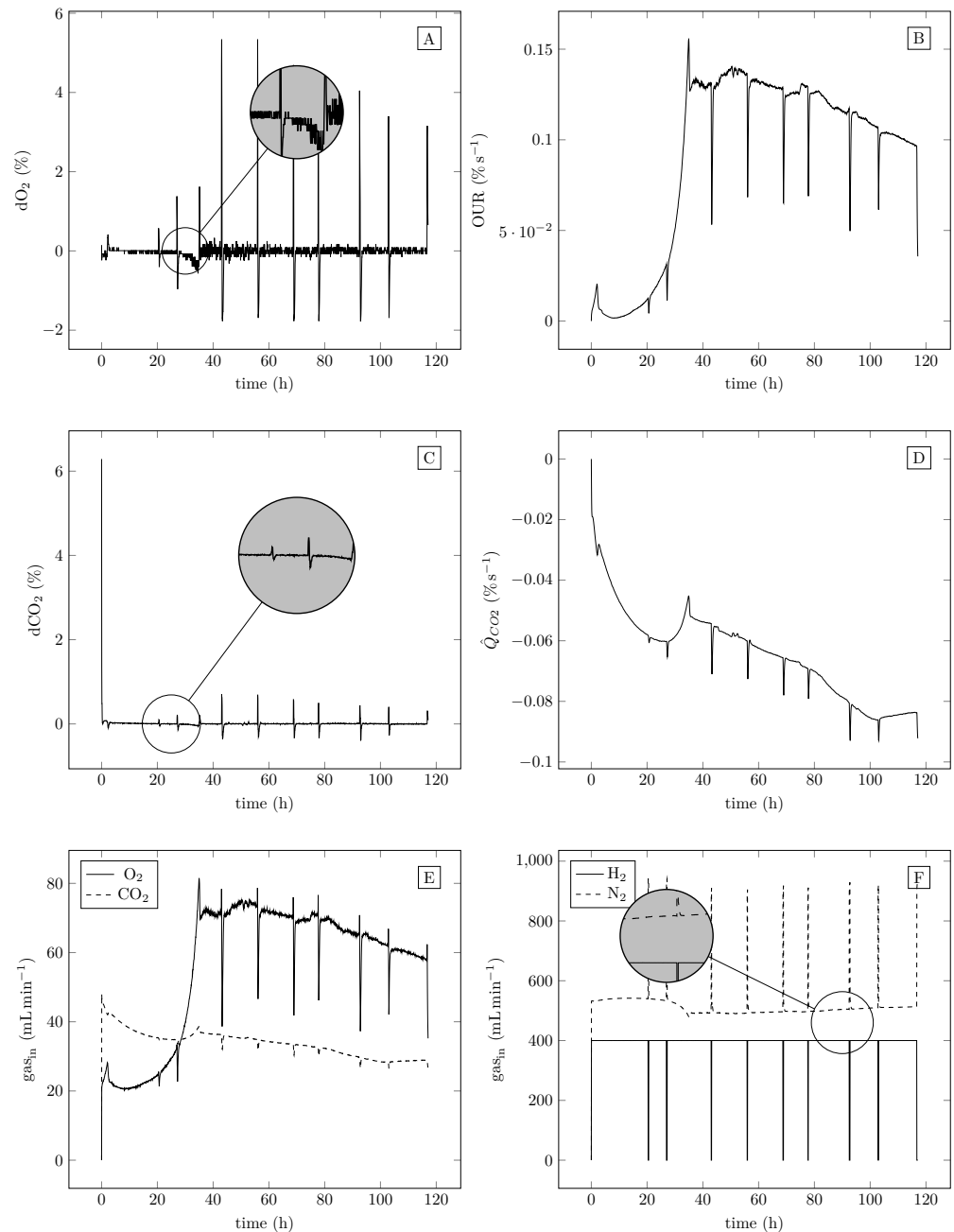


**Figure 5.** Time course of controlled gas fermentation. Panels (A,C) show the evolution of the control errors for O<sub>2</sub> and CO<sub>2</sub>, respectively. Panels (B,D) show the uptake rate estimations for O<sub>2</sub> and CO<sub>2</sub>, respectively. Panel (E) shows the inlet gas flows of O<sub>2</sub> and CO<sub>2</sub>, and panel (F) shows the inlet gas flows of H<sub>2</sub> and N<sub>2</sub>. While O<sub>2</sub>, CO<sub>2</sub> and N<sub>2</sub> flows were automatically applied by the controller, H<sub>2</sub> was switched off manually during sampling.

The bioreactor designed herein (ex-safe with tight control of  $dO_2$ ) allowed for precise adjustment of dissolved oxygen in very low concentration ranges. The effect of 1, 2 and 4%  $dO_2$  on biomass and PHB formation in cultivations of *C. necator* is summarized in Figure 6. The residual biomass in all gas cultivations was  $3.6 \pm 0.2$  g/L. By doubling the oxygen concentration from 2% (0.75 mg/L) to 4% (1.51 mg/L)  $dO_2$ , growth rates

( $\mu_{\max}(2\%) = 0.056$ ,  $\mu_{\max}(4\%) = 0.016$ ) were up to 70% reduced while PHB production rates ( $\mu_{\max\text{PHB}}(2\%) = 0.057$ ,  $\mu_{\max\text{PHB}}(4\%) = 0.038$ ) were 33% reduced (Supplementary Table S2, Figures S3–S5). Reducing the  $dO_2$  from 2% to 1% (0.38 mg/L) slightly lowered the total biomass (20%) and PHB content (8%), while growth and PHB storage rates were approximately the same. With 1%  $dO_2$ , however, the oxygen concentration in the gas phase remained below the lower explosion limit (LEL) throughout the whole gas cultivation. The maximal  $O_2$  concentration in the supply gas was 4% [15]. Although the maximally applied 4%  $O_2$  was below the LEL of 4.8%  $O_2$ , the directives for the minimum safety requirements for workplaces and equipment still applied. A reduction in the  $O_2$  concentration in the gas phase to 50% of the LEL (hence, 2.4%  $O_2$ ) would be required to offset Austrian and European safety regulations (ATEX directives RL 1999/92/EG and RL 2014/34/EU). However, a permanent reduction in the prevailing ex-zone from 0 to 1 or 2 would render the cultivation setup drastically cheaper and lower the explosion risk. The observed high impact of  $dO_2$  on the biomass production (residual biomass plus PHB) might shed a different light on previously published data. Inconstant  $dO_2$  concentrations might have covered effects and led to more complex relationships than assumed.

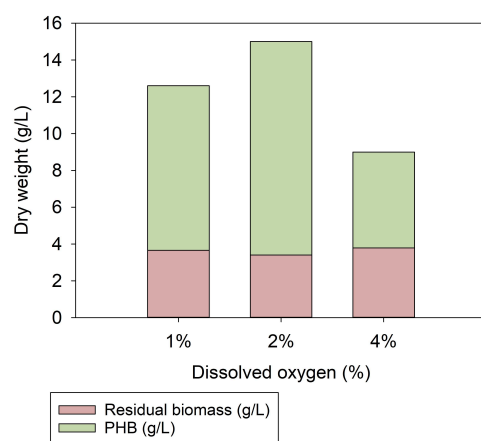


**Figure 6.** Dependence of biomass production on levels of dissolved oxygen.  $dO_2$  concentrations of 1%, 2% and 4% were tested. Doubling the oxygen concentration in the liquid phase from 2% to 4% (1.51 mg/L) reduced the total biomass and therefore the PHB by up to 50%. Reduction of  $dO_2$  from 2% to 1% led to a reduction of 20% in biomass and 5% in PHB. The residual biomass in all fermentations was 3 g/L.

## 5. Discussion

Gas fermentation is an upcoming technology utilizing microorganisms to convert (waste) gases such as  $CO_2$ , CO, syngas or  $CH_4$  into value-added products (platform chemicals, fuels, polymers or amino-acid-rich biomass). Handling gaseous substrates is, in itself, technically difficult. However, it becomes particularly difficult with toxic, flammable or even explosive gases or gas mixtures. In this context, the cultivation of HOBs stands out in particular, as they are efficiently grown on a gas mixture composed of  $CO_2$ ,  $H_2$  and  $O_2$  with  $H_2$  as the main part. The gaseous substrates  $H_2$  and  $O_2$  form explosive oxyhydrogen mixtures within wide mixing ratios (explosion limits of 4.8 and 95.2%  $H_2$ ) and very low minimum ignition energies ( $MIE \geq 0.016$  mJ). Ignition of stoichiometric  $H_2$  and  $O_2$  mixtures ( $H_2:O_2 = 2:1$ ) leads to maximum pressure peaks and pressure rise rates [38]. From a technological point of view, it is therefore advantageous to remain as far below the stoichiometric  $O_2$  concentration as possible—in the best case, below the lower explosion limit of 4.8%  $O_2$ . Therefore, it is important to add just enough  $O_2$  for the growth of microorganisms. Narrow limits for dissolved  $O_2$  were reported for the growth of *C. necator* and PHB formation: for growth, approximately 0.4 to 1.5 mg/mL (corresponding to 1.3 and 4%  $O_2$  saturation) was considered optimal. For PHB production, microbial  $O_2$  demand is considered to be approximately halved (14, 19). Reasons for vague data specifications include, on the one,

hand technical difficulties in fine tuning and precise measurement of very low O<sub>2</sub> concentrations and, on the other hand, the high number of *C. necator* strains used in the literature. High-precision control of O<sub>2</sub> supply is therefore a cornerstone of process safety and of paramount importance from a biological point of view. A low O<sub>2</sub> concentration in the gas phase reduces the probability of an explosion, as well as the explosion pressure in case of an accident (O<sub>2</sub> below the LEL). Automation increases process reliability and reproducibility and reduces manual work at the bioreactor, which constitutes a further level of personal safety and reduced personnel costs.

**Supplementary Materials:** The following supporting information can be downloaded at <https://www.mdpi.com/article/10.3390/fermentation9070619/s1>, Table S1: Comparison of fermentation conditions.; Figure S1: Comparison of two independent fermentations. Figure S2: Comparison of oxygen concentration in gas feed during fermentation.; Table S2: Maximal rate ( $\mu_{max}$ ) of growth, PHB storage and death phase at different dissolved oxygen concentrations of 1, 2 and 4 %. Table S3: All data points from the fermentations. Figure S3: Growth phases and corresponding maximal rates during fermentation with 1% dissolved oxygen.; Figure S4: Growth phases and corresponding maximal rates during fermentation with 2 % dissolved oxygen.; Figure S5: Growth phases and corresponding maximal rates during fermentation with 4 % dissolved oxygen.; Raw data of all fermentations can be found in the corresponding excel file.

**Author Contributions:** Conceptualization, V.L., V.S., M.R. and R.K.; methodology, V.L., A.P., Z.P. and M.R.; software, A.P., Z.P. and M.R.; validation, V.L., A.P. and M.R.; formal analysis, A.P. and M.R.; investigation, V.L.; resources, R.K. and C.H.; data curation, V.L. and A.P.; writing—original draft preparation, V.L., A.P., R.K. and M.R.; writing—review and editing, Z.P., V.S., C.H., R.K. and M.R.; visualization, V.L. and A.P.; supervision, Z.P., V.S., R.K. and M.R.; project administration, V.L., V.S. and R.K.; funding acquisition, C.H. and R.K. All authors have read and agreed to the published version of the manuscript.

**Funding:** The COMET center ACIB: Next Generation Bioproduction was funded by BMK, BMDW, SFG, Standortagentur Tirol, the Government of Lower Austria and the Vienna Business Agency within the framework of COMET—Competence Centers for Excellent Technologies. The COMET-Funding Program was managed by the Austrian Research Promotion Agency FFG (funding number 872161). Role of funding: employment of Vera Lambauer and Alexander Permann, financing cultivation equipment (portable).

**Institutional Review Board Statement:** Not applicable.

**Informed Consent Statement:** Informed consent was obtained from all subjects involved in the study.

**Data Availability Statement:** The data presented in this study are available in Supplementary material.

**Acknowledgments:** We thank TU Graz for supporting our publication through the TU Graz Open Access Publishing Fund. We thank the Faculty of Technical Chemistry, Chemical and Process Engineering, Biotechnology, Graz University of Technology, for providing gas cultivation equipment (non-portable). We thank Markus Raiber, Markus Sackl, Markus Müller and Heinz Strauß from the Institute of Thermal Engineering, Graz University of Technology, for discussions and practical support in H<sub>2</sub> handling and bioreactor setup. We thank Alexander Sigg for process engineering support. We thank Robert Kourist for GC measurements. Open Access Funding by the Graz University of Technology.

**Conflicts of Interest:** The authors declare no conflict of interest. The funders had no role in the design of the study; in the collection, analyses or interpretation of data; in the writing of the manuscript; or in the decision to publish the results.

## Abbreviations

The following abbreviations are used in this manuscript:

CDW	Cell dry weight (g L <sup>-1</sup> )
OD <sub>600</sub>	Optical density at 600 nm
PHB	Poly-(R)-3-hydroxybutyrate

PHA	Polyhydroxyalkanoates
ATEX	Abbreviation from french “atmosphères explosibles” = explosive atmosphere
HOBs	Hydrogen-oxidizing bacteria
MFCs	Mass flow controllers (mL min <sup>-1</sup> )
dO <sub>2</sub>	Dissolved oxygen concentration (%)
dCO <sub>2</sub>	Dissolved carbon dioxide concentration (%)
LEL	Lower explosion limit

## References

- Honegger, M.; Michaelowa, A.; Roy, J. Potential implications of carbon dioxide removal for the sustainable development goals. *Clim. Policy* **2021**, *21*, 678–698. [[CrossRef](#)]
- Hilaire, J.; Minx, J.C.; Callaghan, M.W.; Edmonds, J.; Luderer, G.; Nemet, G.F.; Rogelj, J.; del Mar Zamora, M. Negative emissions and international climate goals-learning from and about mitigation scenarios. *Clim. Chang.* **2019**, *157*, 189–219. [[CrossRef](#)]
- Bistline, J.E.T.; Blanford, G.J. Impact of carbon dioxide removal technologies on deep decarbonization of the electric power sector. *Nat. Commun.* **2021**, *12*, 3732. [[CrossRef](#)]
- Ghiat, I.; Mahmood, F.; Govindan, R.; Al-Ansari, T. CO<sub>2</sub> utilisation in agricultural greenhouses: A novel ‘plant to plant’ approach driven by bioenergy with carbon capture systems within the energy, water and food Nexus. *Energy Convers. Manag.* **2021**, *228*, 113668. [[CrossRef](#)]
- Anwar, M.; Fayyaz, A.; Sohail, N.; Khokhar, M.; Baqar, M.; Yasar, A.; Rasool, K.; Nazir, A.; Raja, M.; Rehan, M.; et al. CO<sub>2</sub> utilization: Turning greenhouse gas into fuels and valuable products. *J. Environ. Manag.* **2020**, *260*, 110059. [[CrossRef](#)]
- Lu, Y.; Yu, J. Comparison analysis on the energy efficiencies and biomass yields in microbial CO<sub>2</sub> fixation. *Process. Biochem.* **2017**, *62*, 151–160. [[CrossRef](#)]
- Köpke, M.; Simpson, S.D. Pollution to products: Recycling of ‘above ground’ carbon by gas fermentation. *Curr. Opin. Biotechnol.* **2020**, *65*, 180–189. [[CrossRef](#)]
- Fackler, N.; Heijstra, B.D.; Rasor, B.J.; Brown, H.; Martin, J.; Ni, Z.; Shebek, K.M.; Rosin, R.R.; Simpson, S.D.; Tyo, K.E.; et al. Stepping on the gas to a circular economy: Accelerating development of carbon-negative chemical production from gas fermentation. *Annu. Rev. Chem. Biomol. Eng.* **2021**, *12*, 439–470. PMID: 33872517. [[CrossRef](#)] [[PubMed](#)]
- Teixeira, L.V.; Moutinho, L.F.; Romão-Dumaresq, A.S. Gas fermentation of C1 feedstocks: Commercialization status and future prospects. *Biofuels Bioprod. Biorefining* **2018**, *12*, 1103–1117. [[CrossRef](#)]
- Kusian, B.; Bowien, B. Organization and regulation of cbb CO<sub>2</sub> assimilation genes in autotrophic bacteria. *FEMS Microbiol. Rev.* **1997**, *21*, 135–155. [[CrossRef](#)] [[PubMed](#)]
- Pohlmann, A.; Fricke, W.F.; Reinecke, F.; Kusian, B.; Liesegang, H.; Cramm, R.; Eitinger, T.; Ewering, C.; Pötter, M.; Schwartz, E.; et al. Genome sequence of the bioplastic-producing “Knallgas” bacterium *Ralstonia eutropha* H16. *Nat. Biotechnol.* **2006**, *24*, 1257–1262. [[CrossRef](#)] [[PubMed](#)]
- Sohn, Y.J.; Son, J.; Jo, S.Y.; Park, S.Y.; Yoo, J.I.; Baritugo, K.A.; Na, J.G.; il Choi, J.; Kim, H.T.; Joo, J.C.; et al. Chemoautotroph *Cupriavidus necator* as a potential game-changer for global warming and plastic waste problem: A review. *Bioresour. Technol.* **2021**, *340*, 125693. .: 10.1016/j.biortech.2021.125693. [[CrossRef](#)] [[PubMed](#)]
- Markl, E. PHB - Bio based and biodegradable replacement for PP: A review. *Nov. Tech. Nutr. Food Sci.* **2018**, *2(4)*, 206–209. [[CrossRef](#)]
- Lambauer, V.; Kratzer, R. Lab-scale cultivation of *Cupriavidus necator* on explosive gas mixtures: Carbon dioxide fixation into polyhydroxybutyrate. *Bioengineering* **2022**, *9*, 204. [[CrossRef](#)]
- Schröder, V. *Explosionsgrenzen von Wasserstoff und Wasserstoff/Methan-Gemischen*; Technical Report; Wirtschaftsverlag NW: Bremerhaven, Germany, 2003.
- Tanaka, K.; Ishizaki, A.; Kanamaru, T.; Kawano, T. Production of poly(D-3-hydroxybutyrate) from CO<sub>2</sub>, H<sub>2</sub>, and O<sub>2</sub> by high cell density autotrophic cultivation of *Alcaligenes eutrophus*. *Biotechnol. Bioeng.* **1995**, *45*, 268–275. .: 10.1002/bit.260450312. [[CrossRef](#)]
- Garrigues, L.; Maignien, L.; Lombard, E.; Singh, J.; Guillouet, S.E. Isopropanol production from carbon dioxide in *Cupriavidus necator* in a pressurized bioreactor. *New Biotechnol.* **2020**, *56*, 16–20. .: 10.1016/j.nbt.2019.11.005. [[CrossRef](#)]
- Sonnleitner, B.; Heinzle, E.; Braunnegg, G.; Lafferty, R.M. Formal kinetics of poly-β-hydroxybutyric acid (PHB) production in *Alcaligenes eutrophus* H 16 and *Mycoplana rubra* R 14 with respect to the dissolved oxygen tension in ammonium-limited batch cultures. *Eur. J. Appl. Microbiol. Biotechnol.* **1979**, *7*, 1–10. [[CrossRef](#)]
- Islam Mozumder, M.S.; Garcia-Gonzalez, L.; Wever, H.D.; Volcke, E.I. Poly(3-hydroxybutyrate) (PHB) production from CO<sub>2</sub>: Model development and process optimization. *Biochem. Eng. J.* **2015**, *98*, 107–116. .: 10.1016/j.bej.2015.02.031. [[CrossRef](#)]
- Juengert, J.; Bresan, S.; Jendrossek, D. Determination of polyhydroxybutyrate (PHB) content in *Ralstonia eutropha* using gas chromatography and Nile red staining. *Bio Protoc.* **2018**, *8*, e2748. [[CrossRef](#)]
- Lewis, W.K.; Whitman, W.G. Principles of gas absorption. *Ind. Eng. Chem.* **1924**, *16*, 1215–1220. [[CrossRef](#)]
- Whitman, W.G. The two film theory of gas absorption. *Int. J. Heat Mass Transf.* **1962**, *5*, 429–433. [[CrossRef](#)]
- Lagneau, V.; Pipart, A.; Catalette, H.. Reactive transport modelling and long term behaviour of CO<sub>2</sub> sequestration in saline aquifers. *Oil Gas Sci. Technol.—Rev. IFP* **2005**, *60*, 231–247. .:2005014. [[CrossRef](#)]

24. Pedersen, O.; Colmer, T.; Sand-Jensen, K. Underwater photosynthesis of submerged plants—Recent advances and methods. *Front. Plant Sci.* **2013**, *4*, 140. [[CrossRef](#)]
25. Doran, P.M. Chapter 10—Mass Transfer. In *Bioprocess Engineering Principles*, 2nd ed.; Doran, P.M., Ed.; Academic Press: London, UK, 2013; pp. 379–444. [[CrossRef](#)]
26. Åström, K.J.; Hägglund, T.; Astrom, K.J. *Advanced PID Control*; ISA—The Instrumentation, Systems, and Automation Society: Research Triangle Park, NC, USA, 2006; Volume 461.
27. Hippe, P. *Windup in Control: Its Effects and Their Prevention*; Springer Science & Business Media: Berlin/Heidelberg, Germany, 2006.
28. Simon, D. *Optimal State Estimation: Kalman, H Infinity, and Nonlinear Approaches*; Wiley-Interscience: Hoboken, NJ, USA, [[CrossRef](#)]
29. Lu, Y.; Yu, J. Gas mass transfer with microbial CO<sub>2</sub> fixation and poly(3-hydroxybutyrate) synthesis in a packed bed bioreactor. *Biochem. Eng. J.* **2017**, *122*, 13–21. [[CrossRef](#)]
30. Milder, R.; Kramer, W.; Doblhoff - Dier, O.; Bayer, K. Strategies for optimal dissolved oxygen (DO) control. *IFAC Proc. Vol.* **1995**, *28*, 292–295. In Proceedings of the 6th International Conference on Computer Applications in Biotechnology (CAB 6), Garmisch-Partenkirchen, Germany, 14–17 May 1995. [[CrossRef](#)]
31. Atlič, A.; Koller, M.; Scherzer, D.; Kutschera, C.; Grillo-Fernandes, E.; Horvat, P.; Chiellini, E.; Braunegg, G. Continuous production of poly([R]-3-hydroxybutyrate) by *Cupriavidus necator* in a multistage bioreactor cascade. *Appl. Microbiol. Biotechnol.* **2011**, *91*, 295–304. [[CrossRef](#)] [[PubMed](#)]
32. Lukey, M.J.; Roessler, M.M.; Parkin, A.; Evans, R.M.; Davies, R.A.; Lenz, O.; Friedrich, B.; Sargent, F.; Armstrong, F.A. Oxygen-tolerant [NiFe]-hydrogenases: The individual and collective importance of supernumerary cysteines at the proximal Fe-S cluster. *J. Am. Chem. Soc.* **2011**, *133*, 16881–16892. [[CrossRef](#)]
33. Milker, S.; Sydow, A.; Torres-Monroy, I.; Jach, G.; Faust, F.; Kranz, L.; Tkatschuk, L.; Holtmann, D. Gram-scale production of the sesquiterpene  $\alpha$ -humulene with *Cupriavidus necator*. *Biotechnol. Bioeng.* **2021**, *118*, 2694–2702. . : 10.1002/bit.27788. [[CrossRef](#)]
34. Nyysölä, A.; Ojala, L.S.; Wuokko, M.; Peddinti, G.; Tamminen, A.; Tsitko, I.; Nordlund, E.; Lienemann, M. Production of endotoxin-free microbial biomass for food applications by gas fermentation of Gram positive H<sub>2</sub>-oxidizing bacteria. *ACS Food Sci. Technol.* **2021**, *1*, 470–479. [[CrossRef](#)]
35. Lai, Y.H.; Lan, J.C.W. Enhanced polyhydroxybutyrate production through incorporation of a hydrogen fuel cell and electro-fermentation system. *Int. J. Hydrog. Energy* **2021**, *46*, 16787–16800. In Proceedings of the SEGT-2019, Bangkok, Thailand, 11–14 December 2019. [[CrossRef](#)]
36. Nangle, S.N.; Ziesack, M.; Buckley, S.; Trivedi, D.; Loh, D.M.; Nocera, D.G.; Silver, P.A. Valorization of CO<sub>2</sub> through lithoautotrophic production of sustainable chemicals in *Cupriavidus necator*. *Metab. Eng.* **2020**, *62*, 207–220. [[CrossRef](#)] [[PubMed](#)]
37. Tanaka, K.; Yoshida, K.; Orita, I.; Fukui, T. Biosynthesis of poly(3-hydroxybutyrate-co-3-hydroxyhexanoate) from CO<sub>2</sub> by a recombinant *Cupriavidus necator*. *Bioengineering* **2021**, *8*, 179. [[CrossRef](#)] [[PubMed](#)]
38. Xing, H.; Yu, R.; Xu, G.; Li, X.; Qiu, Y.; Wang, D.; Li, B.; Xie, L. Theoretical and experimental investigation of explosion characteristics of hydrogen explosion in a closed vessel. *Energies* **2022**, *15*, 8630. [[CrossRef](#)]

**Disclaimer/Publisher’s Note:** The statements, opinions and data contained in all publications are solely those of the individual author(s) and contributor(s) and not of MDPI and/or the editor(s). MDPI and/or the editor(s) disclaim responsibility for any injury to people or property resulting from any ideas, methods, instructions or products referred to in the content.